Puthiyapura, V.K. et al. (2013). $Ru_xNb_{1-x}O2$ catalyst for the oxygen evolution reaction in proton exchange membrane water electrolysers.
International Journal of hydrogen Energy, 38: 8605 – 8616.
http://dx.doi.org/10.1016/j.ijhydene.2013.04.100

$Ru_xNb_{1-x}O2$ catalyst for the oxygen evolution reaction in proton exchange membrane water electrolysers

Vinod Kumar Puthiyapura, Sivakumar Pasupathi, Suddhasatwa Basu, Xu Wu, Huaneng Su, N. Varagunapandiyan, Bruno Pollet and Keith Scott

Abstract:
Bimetallic catalyst system of ruthenium oxide (RuO_2) and niobium oxide (Nb_2O_5) was prepared using the Adams method and the hydrolysis method. Physical and electrochemical characterizations of the catalysts were studied using X-ray diffraction (XRD), Scanning electron microscopy (SEM), cyclic voltammogram (CV) and polarization measurements. Nb_2O_5 addition to RuO_2 was found to increase the stability of RuO_2. In Adams method the sodium nitrate was found to be forming complex with Nb_2O_5 at high temperature reaction. This makes Adams method unsuitable for the synthesis of $RuO_2eNb_2O_5$ bimetallic system. Hydrolysis method on other hand does not have this problem. But a proper mixture of two oxides was not obtained in hydrolysis method. A lower crystallite size for bimetallic system was obtained with Adams method compared to hydrolysis method. RuO_2 prepared by Adams method had higher activity compared to the hydrolysis counterpart in electrolyzer operation with nafion membrane. A cell voltage of 1.62 V was obtained with RuO_2 (A) at 1 A/cm^2. A higher stability for $Ru_{0.8}Nb_{0.2}O_2$(A) compared to RuO_2

1. Introduction

Current energy demand of the world is satisfied mostly by fossil fuels. Unlimited use of fossil fuels, environmental problems due to emissions from fossil fuel combustions (CO_X, NO_X, SO_X C_nH_m, ashes etc) and increasing global demand for energy has led to the search for alternative clean energy resources such as renewable energy [1,2]. In this respect hydrogen is getting more and more attention recently as its one of the cleanest fuel available and emits nothing but only water on combustion. Hydrogen will play an important role in the future energy scenario to form a sustainable energy carrier. But current hydrogen production is mainly dominated by natural gas reforming and is not eco-friendly as it produces greenhouse gases like CO and CO_2 during the process. Water electrolysis is the most sustainable way for the production of hydrogen, but currently only 4% of hydrogen is produced by water electrolysis [3]. Proton exchange membrane water electrolyzer (PEMWE) first developed by General electric Co. in 1966 is the most attractive and

 v.k.puthiyapura@ncl.ac.uk

efficient method for the production of hydrogen from water at low temperature [1]. State of the art PEMWE has disadvantages in terms of cost and efficiency. For example higher over-potential for oxygen evolution reaction (OER) and material component cost (PEM, bi-polar plates and electrocatalyst) are the major limitation associated with PEM-water electrolysers.

IrO_2 and RuO_2 are found to be the most active catalyst for the OER [4]. RuO_2 is widely used material in electrochemical capacitors as well and has very high capacitance value of 150e260 mF/cm^2 [5]. It is widely used in the chlor-alkali industry as dimensionally stable anode (DSA) [6]. The high capacitance value in RuO_2 arises from the *pseudo*-capacitance by the reaction of proton ($H^þ$) on the surface of RuO_2 [5]. Low temperature process is normally preferred for the preparation of high surface area and small particle size RuO_2 polycrystalline material [7]. The metalemetal distance and radius of the cations in RuO_2 are such a way that overlapping of inner d orbital is possible and leading to conductivity in the ruthenium oxides [8]. The Adam's fusion method has been widely used for the preparation of metal oxide since the method was reported in 1923 [9]. Most of the metal oxides reported for electrolysis process are based on DSA technology developed by H. Beer in 1965 for chlor-alkali industry [10].

In DSA type electrodes metal oxides (RuO_2 or IrO_2) are formed on Ti substrates by thermal decomposition of its precursors. However RuO_2 is unstable in the electrolyzer anodic environment and does not have long term stability [11]. Mixtures of RuO_2 and IrO_2 have been studied as anode catalysts and found to have considerable stability and activity [6]. The $Ir_{0.6}Ru_{0.4}O_2$ has been found to show best performance by Marshall et al. [12]. IrO_2eTa_2O_5 electrodes were found to be the most stable among DSA electrodes with 30% Ta_2O_5 [13]. IrO_2 and RuO_2 are expensive materials leading to high cost of electrolyzer systems. Various non-noble metal oxides such as SnO_2, TiO_2, Ta_2O_5 were added to the RuO_2 and IrO_2 in view of increasing activity and stability [6,12,14,15]. Depending upon the effectiveness of mixing different outcome can be obtained in mixed oxides [16]. It may either form a solid solution or simply a fine mixture. Increasing the number of components in the catalyst may also lead to a finer morphology because of poor mixing and can increase the surface area [5,17e19]. Metal oxides with similar structure and proper atomic radii to RuO_2 such as SnO_2, TiO_2 may form solid solution with RuO_2 whereas oxides with different crystal structure such as Nb_2O_5 and Ta_2O_5 may not form solid solution. But there are discrepancies in various reports regarding the solid solution formation. This could be because of different conditions used for the preparation. The proper solution formation depends on various factors such as oxidation and precipitation kinetics of two metal ions, solvent used to mix the precursors, heating rate etc [16]. Also in many cases bimetallic system resulted in a surface richer in one composition than other [16].

First DSA electrode containing Nb_2O_5 was developed by Terezo et al. [15] using the polymeric precursor method. It was found that 70:30 mol% ratio of $Ti/RuO_2eNb_2O_5$ yielded the highest anodic voltammetric charge (thus higher electrochemical active area) and highest stability among the other compositions studied. RuO_2 and Nb_2O_5 were present as two different crystal structures (rutile and orthorhombic) at 600 ^{o} C calcination temperature and Nb_2O_5 was amorphous at calcination temperatures below 500 ^{o} C [15,20]. Crystalline RuO_2 is a good electronic conductor but a very bad proton conductor whereas hydrous Nb_2O_5 on other hand is proton conductor and conductivity depends on the water content [19,21,22]. Adding niobium oxide to RuO_2 will act as network former [19]. Even though the ionic radii of Ru (IV) and Nb (V) are nearly the same its different crystal structure will restrict the formation of solid solution.

Later in a study by Santana et al. [4,23] on DSA type electrode Nb_2O_5 was found to be stabilizing the Ru + Ti + Ce oxide system. They systematically substituted Nb_2O_5 for CeO_2 and found that addition of Nb increased the stability of the catalyst. The effect of calcination temperature, precursor salt, molar ratios of reducing agents of $IrO_2eNb_2O_5$ DSA electrode has also been studied by Santana et al. [20]. Recently Marshall et al. [12] studied the effect of Ta_2O_5 addition to the Ir þ Ru oxide system prepared by the aqueous hydrolysis method. The particle size and resistivity of the catalyst was found to increase with Ta content in $Ir_xTa_{1-x}O_2$. They found that approximately 20 mol% of Ta could be added without compromising the activity and stability of catalyst significantly.

This current study is based upon the hypothesis that a solid-state mixture between the active oxide (RuO_2) and the stabilizing oxide (Nb_2O_5) is the best anode catalyst for acid water electrolysis considering both activity and stability. Nb_2O_5 has a good stabilizing effect similar to Ta_2O_5 but cheaper in cost [24]. Most of the studies in literature on RuO_2- Nb_2O_5 catalyst system were carried out as DSA electrode on Ti support whereby effects of TiO_2 on the properties of the catalyst especially on the stability cannot be neglected. As PEMWE uses powder catalyst system, it is important to study OER activity of the catalyst in membrane electrode assembly (MEA). A major focus is on the effect of the addition of niobium on ruthenium in terms of physical and electrochemical properties. Two preparation methods are also compared namely the Adams method and the hydrolysis method, in an attempt to prepare the optimum ruthenium-niobium mixture.

2. Experimental methods

Ru (III) chloride (Ru content 45e55%) and $NbCl_5$ (99.995 trace metal basis) from Sigma Aldrich were used as Ru and Nb precursors respectively. $NaNO_3$ (99.5% assay) reagent grade from Merck, 2 propanol from Fischer scientific were used as reagent and solvent respectively.

2.1 Electrocatalyst syntheses

2.1.1 Adams fusion method

$RuCl_3$ precursor as required by stoichiometry was dissolved in isopropanol (IP) solvent and stirred for 3 h. To this $NbCl_5$ solution (added as solution in IP) was added as required by the stoichiometry. The total metal concentration was approximately 0.01 M. To this 20 g of finely grounded $NaNO_3$ was added and stirred well for 4-5 h. The solvent was then evaporated slowly in an air oven at 75 ^{0}C. The sample was transferred to a silica crucible and calcined in a muffle furnace at 500 ^{0}C for 1 h. The sample was kept in the furnace until the temperature reached room temperature. During heat treatment the $NaNO_3$ (melting point = 308 ^{0}C) forms a oxidizing melt, dissolves the precursors and react with it to form nitrates as given in Eq. (1) [25]. The excess salt was then dissolved in DI water. The sample was washed and centrifuged using excess DI water and dried in the air oven at 75 ^{0} C overnight. $Ru_xNb_{1-x}O_2$ (x = 1, 0.8, 0.6, 0.4, 0) materials were prepared using this procedure by varying the precursor for required molar ratios of Ru and Nb. The reaction taking place in the Adam's fusion method [9] can be written as,

$$RuCl_3 + 3NaNO_3 \xrightarrow{\Delta} 3NaCl + Ru(NO_3)_3 \quad (1)$$

$$Ru(NO_3)_3 \xrightarrow{\Delta} RuO_2 + 3NO_2\uparrow + \frac{1}{2}O_2\uparrow \quad (2)$$

The advantage of Adam's fusion method is that two of the bi-products formed are gases (NO_2 and O_2) and are released from the system; only solid bi-product is sodium chloride which can be dissolved in water and is separated easily.

2.1.2. Hydrolysis method

The calculated amount of $RuCl_3$ and $NbCl_5$ (as solution in isopropanol) according to the stoichiometry was dissolved in DI water to yield a total metal concentration of 0.01 M. To this, 0.5 M NaOH solution was added. Metal:NaOH molar ratio was maintained as 1:20. This mixture was then heated at 80 ^{0}C with stirring for 1 h. A deep blue colored complex was formed on heating and was precipitated by oxidizing with 1 M HNO_3 added drop wise until pH of solution reaches 7-8, where a controlled precipitation occurred [5]. At pH below 7, the ruthenium species will be present in the solution as ions and at pH above 7, the sodium ion will be present as impurity [5]. The

exact nature of the precipitate is not known [5] but it was assumed to be an *aqua*-hydroxochloro complex [26]. The solution was stirred overnight, centrifuged and heat treated at 400 ^{o} C for 30 min to form an oxide. A temperature of 400 ^{o} C was reported to be giving better performance by other groups [27,28]. The precipitate at higher temperatures above 300 ^{o} C gives anhydrous RuO_2 [5]. Synthesis of Nb_2O_5 by the same method was also attempted. A white jelly precipitate was formed but the precipitate was not very dense and on drying the precipitate completely disappeared. The catalysts prepared by the Adams fusion method are represented as $Ru_xNb_{1-x}O_2$ (A) and those prepared by the hydrolysis method are represented as $Ru_xNb_{1-x}O_2$ (H) throughout this study. Membrane electrode assembly (MEA) was prepared using these catalysts and tested in PEMWE cell.

2.2 Electrocatalyst characterization

2.2.1 Physical characterization

The X-ray diffraction (XRD) analyses of the samples were carried out using a PANalytical X'Pert Pro MPD, (powered by a Philips PW3040/60 X-ray generator and fitted with an X'Celerator) with Cu-Kα radiation (λ = 1.541874 Å). The data were collected over a range of 5-100^{o} 2θ with a step size of 0.0334^{o} 2θ and nominal time per step of 200 s. All scans were carried out in 'continuous' mode using the X'Celerator RTMS detector. Phase identification was carried out by means of the X'Pert accompanying software program PANalytical High Score Plus in conjunction with the ICDD Powder Diffraction File 2 database (1999) and the Crystallography Open Database (September 2011; www.crystallography.net).

Scanning electron microscopy (SEM) and Energy dispersive X-ray spectroscopy (EDX) analyses were carried out in Fei Xl30 Esem-Feg (Environmental Scanning Electron Microscope-Field Emission Gun) at 20 kv for elemental analysis on uncoated samples in low vacuum mode and at 10 kv on gold coated samples in high vacuum mode for the images. The EDX system was a Rontec using Quantax software.

2.2.2. Electrochemical characterization

Voltammetry analyses of the catalysts were conducted using a potentiostat/galavanostat (Aultolab) and a homemade tantalum working electrode (4 mm diameter) which was well polished well with SiC paper (1200, 2400 and 4000 grade) before use. A Ag/AgCl (sat. KCl) and a Pt wire were used as reference and counter electrode respectively. The catalyst ink was prepared by dispersing the catalyst in 0.5 ml solvent (3:2 water: ethanol mixture) containing nafion solution (25 wt.%). The mixture was sonicated in an ultrasonic bath for 30 min before drop casting 10 ml on to the electrode using a micropipette. It was then dried in the air and introduced in the three electrode cell containing 0.5 M H_2SO_4 solution. Nitrogen gas was purged for 15 min before the experiment. A precondition of the electrode was carried out at 100 mV/s for 10 cycles. Cyclic voltammogram (CV) was carried

out starting from higher scan rate of 200 mV/s up to a lower scan rate of 5 mV/s. All potentials in this study are denoted with respect to Ag/AgCl electrode.

Powder conductivity of the sample was measured by pressing the sample in between two copper pistons. The thickness of the powder was measured using a standard micrometer. Resistance of the sample was measured at various thicknesses by passing voltage and measuring current. Conductivity was calculated from the resistance vs. thickness plot.

Membrane Electrode Assembly (MEA) with the commercial and the as prepared catalysts were prepared using the Catalyst Coated Membrane (CCM) method with Nafion® 115 membrane. Hispec Pt/C (40%) and as prepared oxide catalyst were used as cathode and anode catalyst layer respectively. Nafion solution (Sigma Aldrich) was used as ionomer. The electrolysis was carried out in a stainless body cell (4 cm^2 active area) with two titanium porous sinters. Titanium fiber (Bekenit, Japan, thickness 0.3 mm, porosity 60%) and carbon cloth were used as current collector/backing layer on anode and cathode respectively [29]. Pre-heated deionized water from the reservoir was pumped to the cell with the aid of a peristaltic pump at atmospheric pressure and the cell temperature was maintained at 80 ^oC. The polarization curves (V/I) were recorded potentiostatically from +1 V to +2 V using Neware battery testing system (Neware technology Ltd, China).

3. Results and discussion

3.1 Structures and morphologies

The XRD spectra analysis of $Ru_XNb_{1-X}O_2$(A) is given in Fig. 1. The peaks indicate the rutile structure of the catalysts (JCPDS-40-1290). The peaks at 28, 35, 40 and 54^o are RuO_2 (110), (101), (111) and (211) respectively.

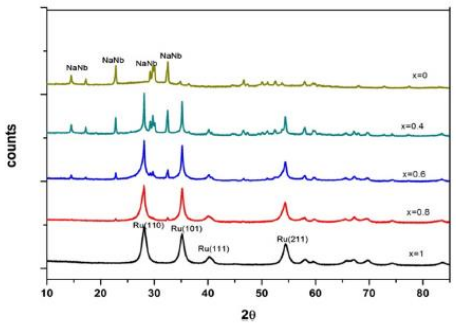

Fig. 1 – XRD spectra of $Ru_xNb_{1-x}O_2$(A) with x value 1,0.8, 0.6, 0.4 and 0.

Table 1 – Average crystallite size of $Ru_xNb_{1-x}O_2$(A) calculated using Scherrer equation from XRD.

x-Value	Crystallite size (nm)			
	t_1	t_2	t_3	$t_{average}$
1	8.27	9.05	8.345	8.55
0.8	10.63	14.12	10.38	11.7
0.6	19.04	22.52	14.635	18.73
0.4	40.9	37.86	27.89	35.55

Peaks at 22.9, 32.59 and 46.7^o started appearing upon Nb_2O_5 addition. These peaks were identified to be $NaNbO_3$ (JCPDS-19-1221) and are represented as NaNb in Fig. 1. This complex formation was due to the reaction between $NaNO_3$ reagent and Nb_2O_5 at high temperature as reported for Nb and Mo elsewhere [30,31].

Peak intensities of $NaNbO_3$ peaks were lower for $Ru_{0.8}N$-$b_{0.2}O_2$(A) and were due to the low weight% of Nb_2O_5 in the catalyst. RuO_2 peaks were clearly visible even in Nb_2O_5 rich compositions and thus can be concluded that RuO_2 was crystallizing well in our experimental conditions and the presence of niobium oxide did not depress crystallization of RuO_2. Crystallinity is higher for RuO_2 as it crystallizes before Nb_2O_5. Since Nb_2O_5 and Ta_2O_5 are amorphous at temperatures below 500 ^{o} C [13,15,20], it can be confirmed that the peaks associated with Nb_2O_5 in the XRD are $NaNbO_3$ (which is formed and crystallized at lower temperature) and not Nb_2O_5. The differences in crystal structure of Nb_2O_5 and RuO_2 will make it difficult to form a solid solution. But in a mixed oxide system, in order to have an influence on catalyst activity, a perfect solid solution formation is not required, but a fine mixing of metals is sufficient [15,32]. In DSA electrodes, IrO_2eTa_2O_5 catalysts were found to be the best catalysts for OER which cannot be explained based on the solid solution formation between the two metal oxides [13,15]. In fact since the RuO_2 and Nb_2O_5 possess two different crystalline structures a tension between the two species is predominantly present at higher crystallinity and this tension tend to increase on Nb_2O_5 crystallization in turn decreasing the catalytic activity [15].

The crystallite sizes of the catalysts were determined using the Scherer's Eq. (3),

$$t = \frac{0.9\lambda}{\beta \cos\theta} \qquad (3)$$

where 't' is the crystallite size, l is the wavelength of the X-ray, b is the full width at half maximum and q is the position of the peak. Three major peaks at 28, 35 and 54^o were used to calculate the average crystallite sizes. The crystallite sizes of $Ru_XNb_{1-X}O_2$ (A)

calculated from XRD are shown in Table 1. The lowest crystallite size was found to be for RuO_2(A) (8e9 nm).

A gradual increase in the crystallite sizes was evident on Nb_2O_5 addition. This is partly because of lack of solid solution formation between Nb_2O_5 and RuO_2 as both have different crystalline structures and partly because of sodiumeniobium complex formation. The crystallite sizes of RuO_2(A) and $Ru_{0.8}Nb_{0.2}O_2$(A) were almost similar (w3 nm difference) due to the low Nb_2O_5 content and thus low $NaNbO_3$. There is a steep increase in crystallite sizes from $Ru_{0.6}Nb_{0.4}O_2$(A) to $Ru_{0.4}$N-$b_{0.6}O_2$(A) due to the higher content of Na(I) ion which has a very large ionic radii compared to Ru(IV) and Nb(V). Lower crystallite sizes may indicate a higher geometric surface area but do not necessarily lead to electrochemical activity since inert Nb_2O_5 dilute the RuO_2 catalyst[14].

In order to study the effect of NaeNb complex formation with respect to temperature, $Ru_{0.8}Nb_{0.2}O_2$(A) composition was selected and was prepared at different calcination temperatures. The XRD plots of these compositions were prepared at various calcinations temperatures are shown in Fig. 2. The increased intensity of RuO_2 peak with increasing calcination temperature indicates the increase in crystallization at high temperature. Variations in the intensity of the peaks of $NaNbO_3$ were very clear as the calcination temperature was increased from 400 ^{0} C to 550 ^{0} C. The $NaNbO_3$ peak started to appear above calcination temperature 450 ^{0} C and thus it can be concluded that $NaNbO_3$ complex formation occurs only above 400 ^{0} C. This behavior is prominent in Adams fusion method as pure $NaNO_3$ is used as oxidizing agent. An increase in crystallite size is also clear with respect to the calcination temperature (Table 2). The increase in crystallite size was smaller from 400 ^{0}C to 450 ^{0} C, but from 450 to 500 ^{0}C a steep increase is observed. This is due to the formation of $NaNbO_3$ complex above 450 ^{0} C as previously explained. It can be assumed that the increase in particle size in rutheniumeniobium mixture here is mainly due to the sodiumeniobium complex more than that of effect of niobium oxide addition to ruthenium oxide.

The XRD spectrum of $Ru_XNb_{1-X}O_2$(H) is given in Fig. 3. The XRD behavior of RuO_2(H) was similar to RuO_2(A). Both shows well-defined rutile structures; however Nb addition gave different patterns in both methods of preparation.

Fig. 3 shows that the intensity of the XRD peaks decreases with decreasing ruthenium content. Also Nb_2O_5 peaks are not visible in any of these spectra which are due to the amorphous nature of Nb_2O_5 at the prepared conditions (400 ^{0} C for 30 min) [20,23]. It is evident that amorphous nature of Nb_2O_5 makes RuO_2 crystallization difficult due to the easily hydrolyzing behavior of Nb_2O_5 [20]. The niobium aqua-hydroxide complex formed during the hydrolysis stage may cover the active sites of ruthenium *aqua*-hydroxide complex

intermediates [26]. The peaks of RuO_2 in Fig. 3 showed amorphous nature (broader peak) at high Nb_2O_5 content.

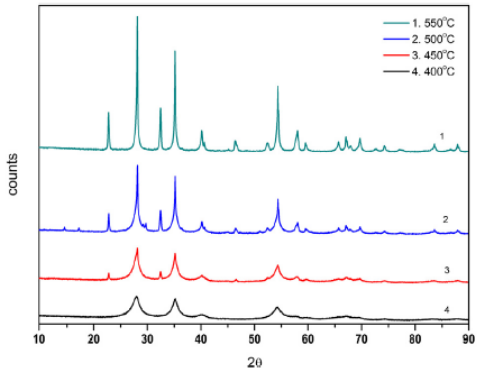

Fig. 2 – XRD spectra of $Ru_{0.8}Nb_{0.2}O_2$(A) prepared at different calcination temperatures.

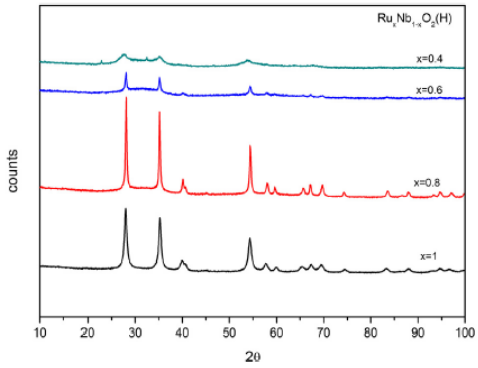

Fig. 3 – XRD of $Ru_xNb_{1-x}O_2$(H) with x value 1, 0.8, 0.6 and 0.4.

Pure Nb_2O_5 was also prepared using hydrolysis method but unfortunately failed as explained in the experimental section. The difficulty in obtaining a precipitate of Nb_2O_5 was reported elsewhere [33]. However the presence of Nb_2O_5 in all other compositions were detected in EDX analyses caused by the precursor of ruthenium acting as a nuclei for the precipitation of Nb_2O_5. Such nuclei are not available when preparing Nb_2O_5. Since in the Adams method no effect on crystallization of RuO_2 was found on Nb_2O_5 addition in XRD, the different hydrolyzing behavior of $NbCl_5$ and $RuCl_3$ could be the reason for the amorphous nature at high niobium content in the hydrolysis method. The small peaks which appear only at higher Nb content ($Ru_{0.4}Nb_{0.6}O_2$) at around 22 and 33^0 are associated to sodiumeniobium complexes formed from the NaOH impurity. Crystallite sizes of the catalysts prepared by hydrolysis method are given in Table 3. The table shows that the crystallite sizes of bimetallic catalyst by Adams method are lower than that of hydrolysis method. The reason for this is not very clear. It cannot be explained based on crystalline nature of the catalyst since hydrolysis method gives more amorphous nature, its crystallite size should be smaller than that in Adams method. Even though in both methods solid solution formation will not occur, a better interaction between the two oxides (or a partial solid solution) is evident in Adams method whereas in hydrolysis method both oxides form simple physical mixtures with lower interaction between them. The large increase in crystallite size for $Ru_xNb_{1-x}O_2$ above 60% Nb_2O_5 addition in Adams fusion method can be mainly attributed to the presence of sodium in the lattice.

Crystallite sizes were found to increase on Nb_2O_5 addition in hydrolysis method as well. $Ru_{0.4}Nb_{0.6}O_2$(H) showed lower crystallite sizes compared to other. The crystallite size of this composition calculated from Scherrer equation may not be accurate since the wide peak in XRD is more likely due to amorphous nature of

the material. The XRD analysis confirms the amorphous nature of the catalyst at higher Nb content. The peaks at ~27° and ~35° are not well resolved at high Nb_2O_5 content indicating that niobium oxide crystallization was not complete at 400 °C. This was also the case in the Adams fusion method but RuO_2 formation was complete even at 400 °C in the hydrolysis method whereby peaks were well resolved unlike in the fusion method. Here a distinction has to be made in both processes as nitrates are the intermediate in the fusion method for decomposition and hydroxides are the intermediates for decomposition in the hydrolysis method. The decomposition of nitrates produces less crystalline RuO_2 [34]. Crystallization in the hydrolysis method was easier than in the fusion method. This could be due to the fact that in the fusion method the oxide formation reaction takes place in many steps, for example (i) dispersion of precursor in $NaNO_3$ (ii) melting of $NaNO_3$ (308 °C) (iii) reaction of the precursor with the melt $NaNO_3$ to form nitrates (iv) decomposition of nitrates to form their respective oxides by releasing NO_2 gas whereas in hydrolysis the overall mechanism is governed by the thermal decomposition of hydroxide which is formed before the calcination stage. The intermediate steps involved in the hydrolysis method are less than that in the fusion method during the oxide formation.

Table 2 – Average crystallite sizes of $Ru_{0.8}Nb_{0.2}O_2$(A) calcined at different temperature.

Calcination temperature (°C)	Crystallite size (nm)			
	t_1	t_2	t_3	$t_{average}$
400	5.31	7.5	6.07	6.29
450	8.62	11.11	8.93	9.55
500	28.23	27.77	22.89	26.23
550	38.98	37.86	28.79	35.21

Table 3 – Average crystallite size of $Ru_xNb_{1-x}O_2$(H) calculated using the Scherrer equation from XRD.

x-Value	Crystallite size (nm)			
	t_1	t_2	t_3	$t_{average}$
1	13.2	13.6	11.74	12.8
0.8	24.076	26.87	27.2	26.04
0.6	24.805	23.14	17.5	21.815
0.4	6.013	10.04	10.98	9.041

3.1.1 Morphology

SEM and TEM techniques were used to observe the morphology of the catalysts. The RuO_2 (A) sample showed well crystalline particle structure. Fine particles can be seen in SEM (Fig. 4a and b). It seems that the particles are more dense and agglomerated. $Ru_{0.8}Nb_{0.2}O_2$ (A) also shows a similar morphology as RuO_2 (A). The hydrolysis method gives more uniform particles compared to Adams method (Fig. 4c and d). The particle size is higher than that of Adams method. The difference in morphology is due to the difference in preparation method. More agglomerated structure in Adams method may be due to the high temperature used for the synthesis. Since temperature used for hydrolysis method here is 400 °C, the formed oxide is likely to contain some amorphous hydrous oxide as well.

3.1.2 Powder conductivity

A linear relationship was observed for the thickness vs. resistance plot (Fig. 5 insert) of the powder sample indicating ohmic behavior of the samples. The

powder conductivity of the sample is shown in Fig. 5. The RuO_2(A) exhibited higher conductivity than RuO_2(H). This is mainly due to the higher crystallinity of the catalysts prepared at 500 ^{o}C compared to RuO_2 (H) prepared at 400 ^{o}C, in other words, a higher crystallinity increases the electronic conductivity of the particle.

However, the electronic conductivity of $Ru_xNb_{1-x}O_2$ prepared by both methods decreases on Nb_2O_5 addition, a sharp decrease in the conductivity was observed for the catalysts prepared by the Adams method than in the hydrolysis method. The higher decrease for the Adams method is caused by the sodium ion in the catalyst. The electronic conductivity in the catalyst is mainly attributed to the RuO_2 network as Nb_2O_5 is an insulator. The presence of non-conducting particles in the catalyst may restrict the electron conduction path in turn increasing the overall resistance of the catalyst layer. This issue is more severe if the two components do not form a solid solution. If a proper solid solution is formed, the overall resistivity of the catalyst is expected to be lower or similar to the conducting component. An effect of calcination temperature on the powder conductivity of $Ru_{0.8}Nb_{0.2}O_2$ (A) is shown in Fig. 6.Contrary to the expected increase, the conductivity values decrease due to the sodiumeniobium complex formation. Above 450 ^{o}C the sodiumeniobium complex starts to form as indicated by XRD (Fig. 2). The conductivity of the compositions prepared at 400 ^{o}C and 450 ^{o}C were similar.

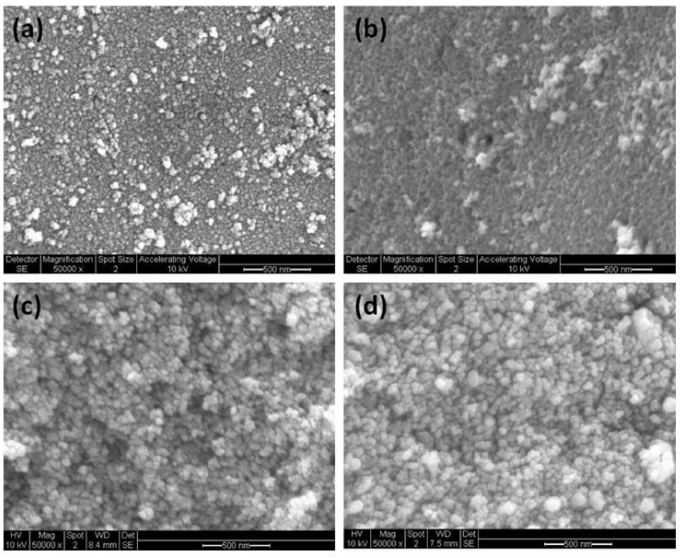

Fig. 4 – SEM picture of (a) RuO_2(A) (b) $Ru_{0.8}Nb_{0.2}O_2$(A) (c) RuO_2(H) (d) $Ru_{0.8}Nb_{0.2}O_2$(H) (magnification 50×K).

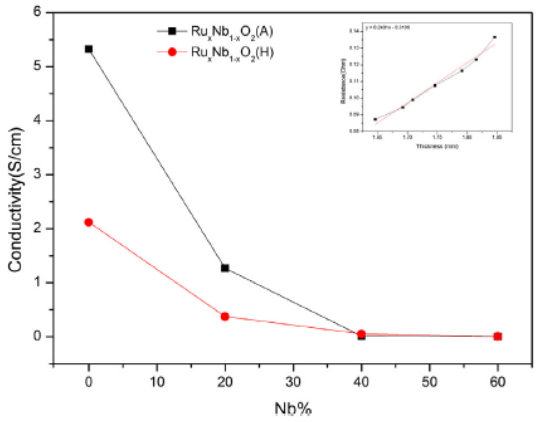

Fig. 5 – Powder conductivity of $Ru_xNb_{1-x}O_2$(A) and $Ru_xNb_{1-x}O_2$(H) as a function of composition. Insert shows the thickness vs. resistance plot for RuO_2(H).

4. Electrochemical characterization

4.1 Cyclic voltammetry

The electrochemical performance of the prepared catalyst samples was tested by cyclic voltammetry. CV of RuO_2 (A) is shown in Fig. 7. The RuO_2(A) shows common shape and features of the rutile RuO_2. A similar shape for crystalline RuO_2 is reported elsewhere [5,35]. The broad peaks are characteristic of metal oxides with no well-defined double layer region. The peaks at around þ0.4 V and þ1.0 V (vs. Ag/AgCl) are commonly attributed to the Ru (III)/Ru(IV) and Ru(IV)/Ru(V) surface transitions respectively [30,36] due to the redox charge transition between the hydrogen ion ($H^þ$) and RuO_2 surface [8,37] as shown below,

$$RuO_x(OH)_y + \delta H^+ + \delta e^- \leftrightarrows RuO_{x-\delta}(OH)_{y+\delta} \qquad (4)$$

For all compositions current density decreased with scan rate. The characteristic redox peaks of RuO_2 disappeared on Nb_2O_5 addition. A similar behavior was also reported for DSA type electrode [15]. Oxygen evolution currents were also suppressed on Nb_2O_5 addition. The RuO_2(A) and $Ru_{0.8}N\text{-}b_{0.2}O_2$(A) sample potentiodynamic curves were almost symmetrical around zero current indicating that they act as capacitor. Lower activity above 20% Nb_2O_5 is due to the dilution of RuO_2 by Nb_2O_5 and the sodiumeniobium complex formation. Capacitance values were calculated from,

$$C = i/(dE/dt) \qquad (5)$$

where i is the current and dE/dt is the scan rate[13]. Since in metal oxide double layer capacitance and *pseudo*-capacitance coexist, it is difficult to differentiate between the two[13]. Thus the calculated capacitance C includes both the double layer and *pseudo*-capacitance contribution. The current density at þ0.65 V (vs. Ag/AgCl) where no redox reaction occur is used to calculate capacitance. Here, it

was found that the specific capacitance of RuO_2 (A) and $Ru_{0.8}Nb_{0.2}O_2$ (A) were similar (50.24 F g^{-1}) for our experimental condition. A similar behavior on Nb_2O_5 addition to RuO_2 was reported by Brumbach et al.[19] whereas Terezzo et al. [15] reported an increase in anodic charge on 30% Nb_2O_5 addition to RuO_2. This was explained to the optimized interconnection of the proton conducting Nb_2O_5 and the electron conducting RuO_2 as well as the morphological changes on Nb_2O_5 addition [15,19]. Since Nb_2O_5 is an electronic insulator the current values in CV is solely due to the RuO_2 network [4,15,19]. As it can be observed from the powder conductivity studies the electronic conduction of $Ru_xNb_{1-x}O_2$ (A) conductivity decreases on Nb_2O_5 addition (Fig. 5) and thus the capacitance behavior can not only be explained on the basis of electronic conduction. The amorphous nature and lower electronic conduction of Nb_2O_5 could be the reason for the asymmetric distortion of the CV curves on Nb_2O_5 addition [19]. The formed Nb_2O_5 partially covers the active RuO_2 sites restricting the proton diffusion which is clear from the CVs as the Faradaic peaks at +0.4 and +0.7 V vs. Ag/AgCl disappear on Nb addition. The distortion of the symmetry of the curves is more pronounced at Nb_2O_5 percentage of above 20%. We assume that an optimized interconnection between the RuO_2 and amorphous Nb_2O_5 (or a partial solid solution formation) gives $Ru_{0.8}Nb_{0.2}O_2$ (A), the ideal capacitor behavior and similar capacitance to RuO_2(A). Lower RuO_2 content and the presence of sodium ion in the catalyst reduces the specific capacitance of the catalyst above 20% Nb_2O_5[5].

In order to avoid sodiumeniobium complex formation, a hydrolysis method was adopted for synthesis. Since hydroxides are intermediates in hydrolysis method, a lower temperature (400 ^{o} C) is used for the calcination. Hydroxides require lower calcination temperature for decomposition as clear from XRD. The CV curve at different composition of $Ru_xNb_{1-x}O_2$(H) prepared by hydrolysis method is given in Fig. 8. The trend of CV curve with respect to composition was same as that in Adams method. Redox peaks of RuO_2 are clear in RuO_2(H) as well. On adding Nb_2O_5, the characteristic peaks are lost as in Adams method. The characteristic redox peaks of RuO_2 are clearer in the Adams method due to higher crystallinity [5]. The rectangular shape obtained for $Ru_{0.8}Nb_{0.2}O_2$ (A) was not observed in hydrolysis method and may be due to the lack of proper interaction between RuO_2 and Nb_2O_5 unlike in Adams method.

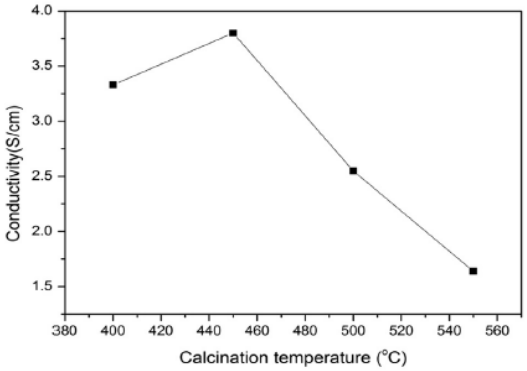

Fig. 6 – Powder conductivity of $Ru_{0.8}Nb_{0.2}O_2$(A) prepared at various calcinations temperature.

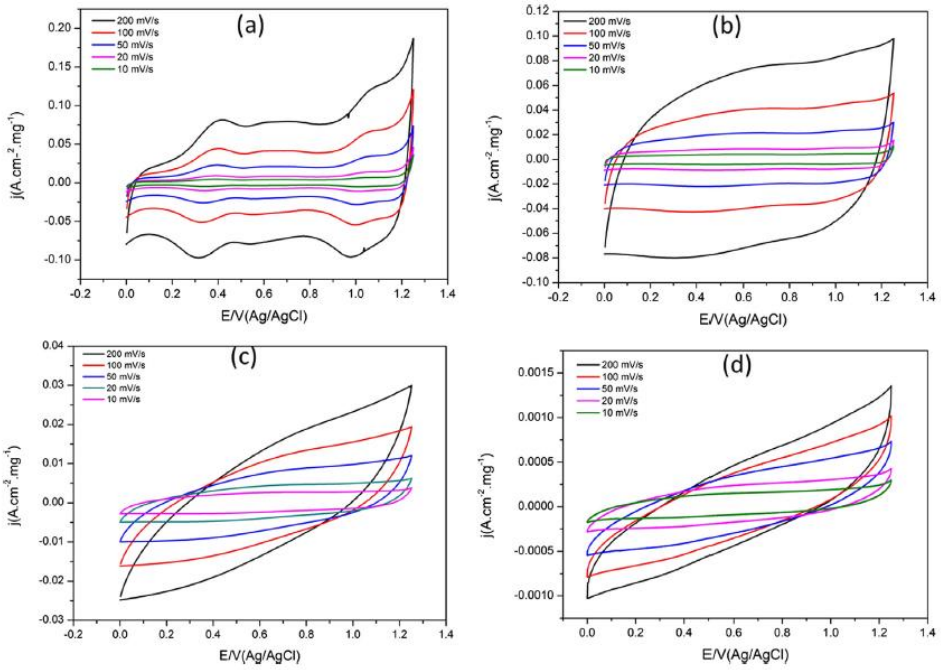

Fig. 7 – CV of $Ru_xNb_{1-x}O_2$(A) with respect to scan rate. (A) RuO_2 (B) $Ru_{0.8}Nb_{0.2}O_2$ (C) $Ru_{0.6}Nb_{0.4}O_2$ (D) $Ru_{0.4}Nb_{0.6}O_2$ in 0.5 M H_2SO_4.

The lower interaction in hydrolysis method can be either due to the lower calcination temperature or due to the different hydrolyzing behavior of $NbCl_5$ and $RuCl_3$. $NbCl_5$ is an easily hydrolyzing salt compared to $RuCl_3$ and in a mixture of both, the former hydrolyzes first and the positively charged niobium ions interact with the $RuCl_3$ preventing the complete oxidation of ruthenium. RuO_2 formed thus will not be crystallized very well at the prepared condition [20].

The specific capacitance of RuO_2(H) and $Ru_{0.8}Nb_{0.2}O_2$(H) were 62.8 F/g and 12.56 F/g respectively. As explained by Zhang et al. the capacitance value is higher for RuO_2 prepared at lower calcination temperatures which could explain the higher capacitance of RuO_2 (H) [5]. The difference in capacitance is very high on adding 20% Nb_2O_5

addition unlike in Adams method. This can be due to the lack of proper interaction between RuO_2 and Nb_2O_5 in the catalyst as explained above.

In order to study the effect of calcinations temperature on performance of $Ru_{0.8}Nb_{0.2}O_2$ (A), a set of catalyst calcined at different temperature of 400, 450, 500 and 550 ^{0} C were prepared. The cyclic voltammogram of which is compared in Fig. 9. The characteristic peaks of RuO_2 starts appearing at calcination temperature of 450 ^{0}C and 500 ^{0} C. A well-defined redox peaks are clearly seen on the samples prepared at 450 ^{0} C and 500 ^{0} C. Interestingly a steep change in the shape and active area can be seen for sample prepared at 550 ^{0} C. A change in shape of CV curve with respect to calcinations temperature was reported for RuO_2 and IrO_2 [5,38] and a decrease in active area with respect to calcinations temperature was reported. A higher calcination temperature increases the crystallinity and clear peaks were expected. The lower active sites for the samples prepared above 500 ^{0} C is partly due to the sintering of particles and partly due to the sodiumeniobium complex formation at this temperature which was clear from XRD peak (Fig. 2). Sintering of particle lead to increase in grain size (Table 2) and thus decrease in active area. As explained in Section 3.1 at high temperature both RuO_2 and Nb_2O_5 crystallizes and increased tension between the two decreasing the active area.

5. Stability of the catalyst

The stability of the catalyst was assessed using continuous CV within the potential range +0 to +1.25 V (vs. Ag/AgCl) and data are shown in Fig. 10. The capacitance as well as the OER current decreases after several cycles of potential scans. This is caused by the dissolution of RuO_2 at high anodic potential to form RuO_4 which dissolves in the solution [36]. The characteristic peaks of RuO_2 are lost after few potential cycles and the decrease in current is gradual with cycles. The loss of characteristic peaks of RuO_2 after a few cycles clearly indicates the dissolution of the RuO_2. An addition of Nb_2O_5 was found to stabilize the RuO_2 in both synthesis methods. The decrease in oxygen evolution current was lower on Nb_2O_5 addition compared to pure RuO_2. Also the effect of Nb_2O_5 addition to the stability was prominent in Adams method than in hydrolysis (Table 4).

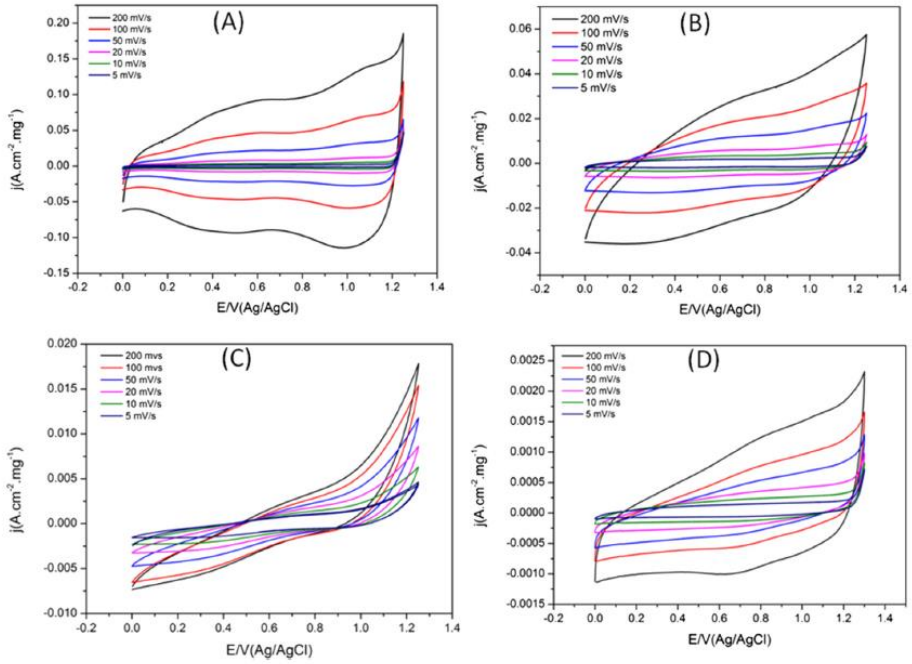

Fig. 8 – CV of $Ru_xNb_{1-x}O_2$(H) with respect to scan rate. (A) RuO_2 (B) $Ru_{0.8}Nb_{0.2}O_2$ (C) $Ru_{0.6}Nb_{0.4}O_2$ (D)$Ru_{0.4}Nb_{0.6}O_2$ in 0.5 M H_2SO_4.

This confirms the better mixture formation in Adams method. This clearly indicates the importance of proper mixture (or partial solid solution) formation between RuO_2 and Nb_2O_5 in order to modify the electrochemical properties of the bimetallic system. The higher stability on adding Nb_2O_5 is an interesting feature as the stability of the catalyst during oxygen evolution is an important drawback of RuO_2 catalyst under water electrolysis operations. In this study, an MEA was fabricated in order to investigate the behavior of the catalyst in 'real' electrolyzer operations.

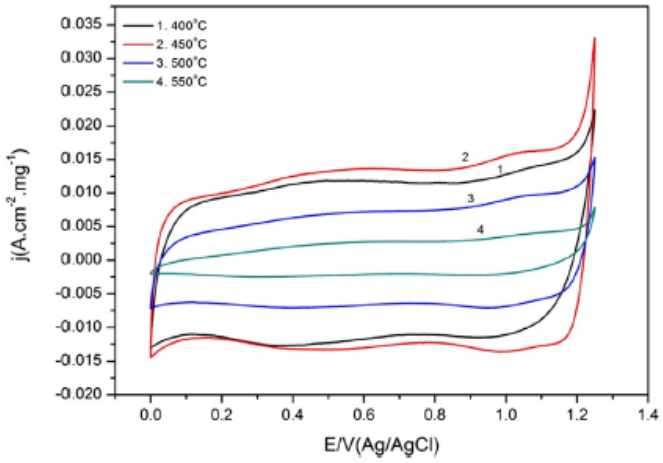

Fig. 9 – CV of $Ru_{0.8}Nb_{0.2}O_2$(A) prepared at different calcination temperature in 0.5 M H_2SO_4 at 20 mV/s.

6. Water electrolysis performance

The MEA performance of the prepared catalyst is shown in Fig. 11. It was found that RuO_2(A) gives the best performance (1.62 V at 1 A cm^{-2}) among all the MEA prepared. The lower performance of $Ru_{0.8}Nb_{0.2}O_2$ (A) may be due to the complex formation of sodium and niobium and also due to the lower electronic conductivity. It was clear from the powder conductivity data that the difference between conductivity of RuO_2 (A) and $Ru_{0.8}Nb_{0.2}O_2$ (A) was more than that of the hydrolysis counterpart. This difference was also shown in the MEA performance. The lower electronic conductivity of the catalyst layer will increase the ohmic drop. No considerable difference in performance was found for RuO_2 (H) and $Ru_{0.8}Nb_{0.2}O_2$(H). A difference of 133 mV at 1 A/cm^2 was found for RuO_2 (A) and RuO_2 (H). From XRD and conductivity it was clear that RuO_2 (H) has higher crystallite size and lower conductivity than RuO_2 (A). This contributes to the lower performance of RuO_2 (H).

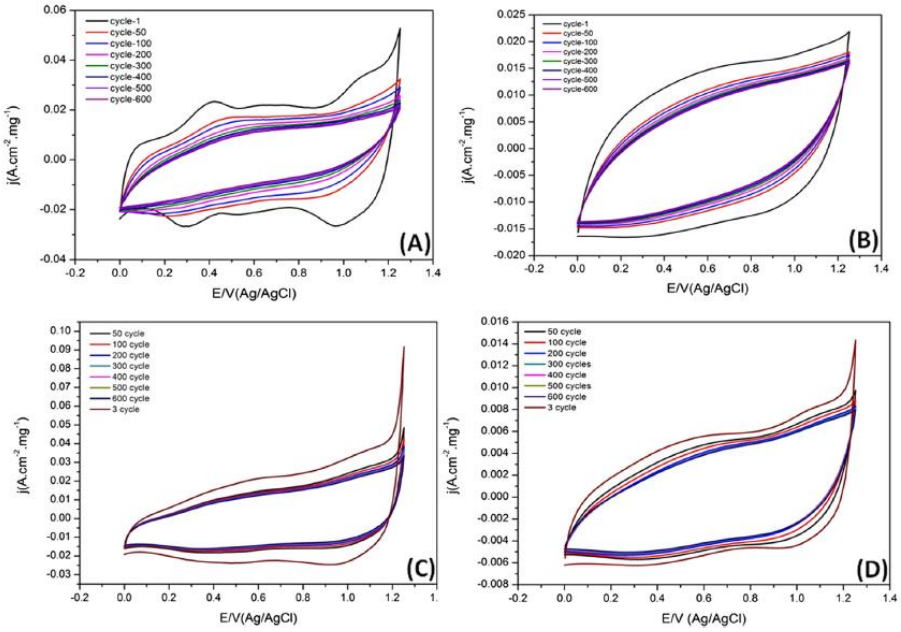

Fig. 10 – Stability of the catalysts (A) RuO_2(A), (B) $Ru_{0.8}Nb_{0.2}O_2$(A), (C) RuO_2(H), (D) $Ru_{0.8}Nb_{0.2}O_2$(H).

However the stability of the MEA with $Ru_{0.8}Nb_{0.2}O_2$ (A) was higher than that of RuO_2 (A) after 23 h electrolysis operation using an MEA at 1 A/cm^2 current density (Fig. 12). It was also observed that the RuO_2 (A) over-potential increases drastically after 20 h of operation whereas $Ru_{0.8}Nb_{0.2}O_2$ (A) shows relatively better performance. The potential value in Fig. 12 is higher than that the one given in Fig. 11. The reason for the higher potential is that the MEA was tested after the polarization up to 2 V and the titanium current collector oxidized to non-conducting titanium oxide. This increased the resistance and thus Ohmic voltage drop. But it is still interesting to note that $Ru_{0.8}Nb_{0.2}O_2$(A) started at higher potential (w2 V)

and maintained that potential almost stable even after 23 h operation whereas RuO_2 (A) started at 1.8 V, increases the potential after about 20 h of operation at 1 A/cm^2 current density.

Table 4 – The stability of RuO_2(A) and $Ru_{0.8}Nb_{0.2}O_2$(A) from continuous cyclic voltammogram.

Catalyst	j(0.4 V) 600th cycle – j(0.4 V) 3rd cycle (A cm^{-2}.mg^{-1})	j(1 V) 600th cycle – j(1 V) 3rd cycle (A cm^{-2}.mg^{-1})
RuO_2 (A)	1.674×10^{-2}	1.8261×10^{-2}
$Ru_{0.8}Nb_{0.2}O_2$ (A)	6.08×10^{-3}	4.38×10^{-3}
RuO_2(H)	6.922×10^{-3}	1.225×10^{-2}
$Ru_{0.8}Nb_{0.2}O_2$ (H)	2.557×10^{-3}	1.55×10^{-3}

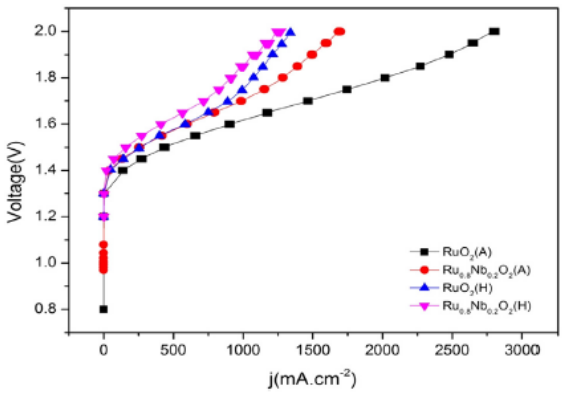

Fig. 11 – MEA performance of $Ru_xNb_{1-x}O_2$(A) and $Ru_xNb_{1-x}O_2$(H) as anode catalyst. Nafion-115 membrane, Pt/C(40%) cathode.

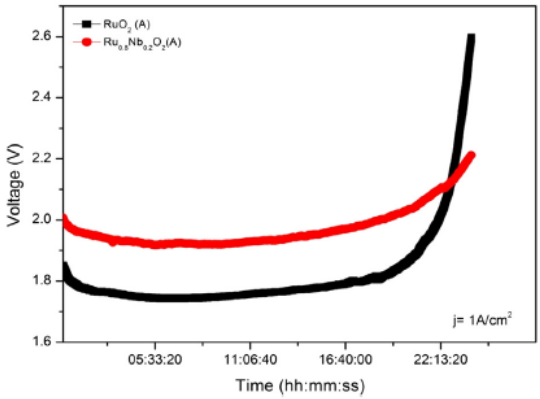

Fig. 12 – MEA stability test of RuO_2(A) and $Ru_{0.8}Nb_{0.2}O_2$(A).

7. Conclusion

A bimetallic $RuO_2eNb_2O_5$ catalyst was prepared as an anode catalyst for oxygen evolution reaction using Adams and hydrolysis methods. The Adams method was found to form a sodiumeniobium complex during synthesis at temperature above 400 ^{0}C. This makes Adams

method unsuitable for the synthesis of RuO_2eNb_2O_5 bimetallic catalyst system. It is assumed that in the Adams method RuO_2 forms a better mixture with Nb_2O_5 (or a partial solid solution) and influence its electrochemical properties. A higher stability was found on adding 20% Nb_2O_5 to RuO_2(A). No enhancement in activity was found due to the dilution of the active component. The increase in stability was more in the Adams method than the hydrolysis method. The hydrolysis method does not have issue of unwanted complex formation, but in this method the Nb intermediate was found to cover the RuO_2 active sites during synthesis due to the easily hydrolyzing nature of $NbCl_5$ precursor. A proper solid solution was not formed in hydrolysis method. In both methods an addition of more than 20% Nb_2O_5 lowered the electronic conductivity and activity of the catalyst. No considerable influence on stability and activity was found on adding 20% Nb_2O_5 to RuO_2 in hydrolysis method. This indicates the importance of partial solid solution (or better mixture) formation between RuO_2 and Nb_2O_5 for modifying the electrochemical properties of RuO_2. $Ru_{0.8}Nb_{0.2}O_2$(A) prepared at different calcinations temperature indicate that sodiumeniobium complex formation decrease the activity of the catalyst significantly.

Acknowledgments

The author acknowledges the financial support from EPSRC (grant reference EP/G042012/1) and UKIERI. We also acknowledge the Advanced Chemical and Materials Analysis (ACMA), Newcastle University for the SEM and XRD analysis.

References

[1] Ma L, Sui S, Zhai Y. Investigations on high performance proton exchange membrane water electrolyzer. International Journal of Hydrogen Energy 2009;34(2):678-84.

[2] Momirlan M, Veziroglu TN. Current status of hydrogen energy. Renewable and Sustainable Energy Reviews 2002;6(1e2):141-79.

[3] Dunn S. Hydrogen futures: toward a sustainable energy system. International Journal of Hydrogen Energy 2002;27(3):235-64.

[4] Santana MHP, De Faria LA. Oxygen and chlorine evolution on RuO_2 + TiO_2 + CeO_2 + Nb_2O_5 mixed oxide electrodes. Electrochimica Acta 2006;51(17):3578-85.

[5] Zheng JP, Cygan PJ, Jow TR. Hydrous ruthenium oxide as an electrode material for electrochemical capacitors. Journal of The Electrochemical Society 1995;142(8):2699-703.

[6] Kö tz R, Stucki S. Stabilization of RuO_2 by IrO_2 for anodic oxygen evolution in acid media. Electrochimica Acta 1986;31(10):1311-6.

[7] Kung HH. Transition metal oxides: surface chemistry and catalysis. In: Delmon B, Yates JT, editors. Studies in surface science and catalysis, Vol. 45. Elsevier; 1989.

[8] Trasatti S, Buzzanca G. Ruthenium dioxide: a new interesting electrode material. Solid state structure and electrochemical behaviour. Journal of Electroanalytical Chemistry and Interfacial Electrochemistry 1971;29(2):A1-5.

[9] Adams R, Shriner RL. Platinum oxide as a catalyst in the reduction of organic compounds. III. Preparation and properties of the oxide of platinum obtained by the fusion of chloroplatinic acid with sodium nitrate. Journal of the American Chemical Society 1923;45(9):2171-9.

[10] Beer HB. The invention and industrial development of metal anodes. Journal of The Electrochemical Society 1980;127(8):303C-7C.

[11] Sedlak JM, Lawrance RJ, Enos JF. Advances in oxygen evolution catalysis in solid polymer electrolyte water electrolysis. International Journal of Hydrogen Energy 1981;6(2):159-65.

[12] Marshall AT, Sunde S, Tsypkin M, Tunold R. Performance of a PEM water electrolysis cell using $Ir_xRu_yTa_zO_2$ electrocatalysts for the oxygen evolution electrode. International Journal of Hydrogen Energy 2007;32(13):2320-4.

[13] Comninellis C, Vercesi GP. Characterization of DSA-type oxygen evolving electrodes: choice of a coating. Journal of Applied Electrochemistry 1991;21(4):335-45.

[14] Wu X, Tayal J, Basu S, Scott K. Nano-crystalline $Ru_xSn_{1-x}O_2$ powder catalysts for oxygen evolution reaction in proton exchange membrane water electrolysers. International Journal of Hydrogen Energy 2011;36(22):14796-804.

[15] Terezo AJ, Pereira EC. Preparation and characterization of Ti/ RuO_2-Nb_2O_5 electrodes obtained by polymeric precursor method. Electrochimica Acta 1999;44(25):4507-13.

[16] Gaudet J, Tavares AC, Trasatti S, Guay D. Physicochemical characterization of mixed RuO_2-SnO_2 solid solutions. Chemistry of Materials 2005;17(6):1570-9.

[17] Sergio T. Physical electrochemistry of ceramic oxides. Electrochimica Acta 1991;36(2):225-41.
[18] Marshall A, Tsypkin M, Borresen B, Hagen G, Tunold R. Nanocrystalline $Ir_xSn_{1-x}O_2$ electrocatalysts for oxygen evolution in water electrolysis with polymer electrolyte e effect of heat treatment. Journal of New Materials for Electrochemical Systems 2004;7(3):197-204.
[19] Brumbach MT, Alam TM, Nilson RH, Kotula PG, McKenzie BB, Tissot RG, et al. Ruthenium oxide-niobium hydroxide composites for pseudocapacitor electrodes. Materials Chemistry and Physics 2010;124(1):359-70.
[20] Santana MHP, De Faria LA, Boodts JFC. Investigation of the properties of Ti/[IrO_2-Nb_2O_5] electrodes for simultaneous oxygen evolution and electrochemical ozone production, EOP. Electrochimica Acta 2004;49(12):1925-35.
[21] Kishimoto A, Kudo T, Nanba T. Amorphous tantalum and niobium oxide proton conductors derived from respective peroxo polyacids. Solid State Ionics 1992;53e56(Part 2):993-7.
[22] Slade RCT, Barker J, Halstead TK. Protonic conduction and diffusion in the hydrous oxides $V_2O_5.nH_2O$, $Nb_2O_5.nH_2O$, $Ta_2O_5.nH_2O$ and $CeO_2.nH_2O$. Solid State Ionics 1987;24(2):147-53.
[23] Santana MHP, Da Silva LM, De Faria LA. Investigation of surface properties of Ru-based oxide electrodes containing Ti, Ce and Nb. Electrochimica Acta 2003;48(13):1885-91.
[24] Terezo AJ, Pereira EC. Fractional factorial design applied to investigate properties of Ti/IrO_2-Nb_2O_5 electrodes. Electrochimica Acta 2000;45(25e26):4351e8.
[25] Hutchings R, Mu¨ ller K, Ko¨ tz R, Stucki S. A structural investigation of stabilized oxygen evolution catalysts. Journal of Materials Science 1984;19(12):3987-94.
[26] Roginskaya YE, Morozova OV. The role of hydrated oxides in formation and structure of DSA-type oxide electrocatalysts. Electrochimica Acta 1995;40(7):817-22.
[27] Ioroi T, Kitazawa N, Yasuda K, Yamamoto Y, Takenaka H. Iridium oxide/platinum electrocatalysts for unitized regenerative polymer electrolyte fuel cells. Journal of The Electrochemical Society 2000;147(6):2018-22.
[28] da Silva LA, Alves VA, da Silva MAP, Trasatti S, Boodts JFC. Oxygen evolution in acid solution on IrO_2 þ TiO_2 ceramic films. A study by impedance, voltammetry and SEM. Electrochimica Acta 1997;42(2):271-81.
[29] Su H, Bladergroen BJ, Pasupathi S, Linkov V, Ji S. Performance investigation of membrane electrode assemblies for hydrogen production by solid polymer electrolyte water electrolysis. International Journal of Electrochemical Science 2012;7(5):4223-34.
[30] Cheng J, Zhang H, Ma H, Zhong H, Zou Y. Preparation of $Ir_{0.4}Ru_{0.6}Mo_xO_y$ for oxygen evolution by modified Adams' fusion method. International Journal of Hydrogen Energy 2009;34(16):6609-13.

[31] Robin A. Corrosion behaviour of niobium in sodium hydroxide solutions. Journal of Applied Electrochemistry 2004;34(6):623-9.
[32] Faria LA, Boodts JFC, Trasatti S. Electrocatalytic properties of ternary oxide mixtures of composition $Ru_{0.3}Ti_{(0.7-x)}Ce_xO_2$ oxygen evolution from acidic solution. Journal of Applied Electrochemistry 1996;26(11):1195-9.
[33] Alquier C, Vandenborre MT, Henry M. Synthesis of niobium pentoxide gels. Journal of Non-crystalline Solids 1986;79(3):383-95.
[34] Ardizzone S, Falciola M, Trasatti S. Effect of the nature of the precursor on the electrocatalytic properties of thermally prepared ruthenium oxide. Journal of The Electrochemical Society 1989;136(5):1545-50.
[35] Arikado T, Iwakura C, Tamura H. Electrochemical behaviour of the ruthenium oxide electrode prepared by the thermal decomposition method. Electrochimica Acta 1977;22(5):513-8.
[36] Song S, Zhang H, Ma X, Shao Z, Baker RT, Yi B. Electrochemical investigation of electrocatalysts for the oxygen evolution reaction in PEM water electrolyzers. International Journal of Hydrogen Energy 2008;33(19):4955-61.
[37] Ardizzone S, Fregonara G, Trasatti S. "Inner" and "outer" active surface of RuO_2 electrodes. Electrochimica Acta 1990;35(1):263-7.
[38] Rasten E, Hagen G, Tunold R. Electrocatalysis in water electrolysis with solid polymer electrolyte. Electrochimica Acta 2003;48(25-26):3945-52.